A&A 411, L81–L84 (2003)
DOI: 10.1051/0004-6361:20031171

Astronomy & Astrophysics

Monte Carlo simulations and generation of the SPI response⋆

S. J. Sturner[1,2], C. R. Shrader[1,2], G. Weidenspointner[1,2,3], B. J. Teegarden[1], D. Attié[4], B. Cordier[4], R. Diehl[5], C. Ferguson[6], P. Jean[3], A. von Kienlin[5], Ph. Paul[3], F. Sánchez[7], S. Schanne[4], P. Sizun[4], G. Skinner[3], and C. B. Wunderer[5]

[1] Code 661, NASA/Goddard Space Flight Center, Greenbelt, MD 20771, USA
[2] Universities Space Research Association, 7501 Forbes Blvd. #206, Seabrook, MD 20706, USA
[3] Centre d'Étude Spatiale des Rayonnements, BP 4346, 31028 Toulouse Cedex 4, France
[4] DSM/DAPNIA/Service d'Astrophysique, CEA Saclay, 91191 Gif-sur-Yvette, France
[5] Max-Planck-Institut für extraterrestrische Physik, Giessenbachstr. 1, 85748 Garching, Germany
[6] Dept. of Physics and Astronomy, University of Southampton, Southampton, S017 1BJ, UK
[7] CSIC-UV, Edificio Institutos de Paterna, Instituto de Física Corpuscular, PO Box 22085, 46071, Valencia, Spain

Received 10 July 2003 / Accepted 31 July 2003

Abstract. In this paper we discuss the methods developed for the production of the INTEGRAL/SPI instrument response. The response files were produced using a suite of Monte Carlo simulation software developed at NASA/GSFC based on the GEANT-3 package available from CERN. The production of the INTEGRAL/SPI instrument response also required the development of a detailed computer mass model for SPI. We discuss our extensive investigations into methods to reduce both the computation time and storage requirements for the SPI response. We also discuss corrections to the simulated response based on our comparison of ground and inflight calibration data with MGEANT simulations.

Key words. INTEGRAL – SPI – gamma rays – methods: data analysis – methods: numerical

1. Introduction

In this paper we discuss the work that has gone into the production of the Spectrometer for INTEGRAL (SPI) instrument response matrices. We discuss the use of the SPI instrumental calibration to evaluate the accuracy of the simulation software and the SPI computer mass model developed at NASA/GSFC. The methods that we have tested and implemented to produce response matrices with sufficient angular and energy resolution within reasonable limitations of computation and storage resources are then described. This is followed by a discussion of the use of SPI ground and flight calibration results to produce correction tables in order to correct inaccuracies inherent to simulated responses.

2. Simulations and the SPI mass model

SPI went through an extensive ground calibration campaign during April 2001 at the Commissariat à l'Énergie Atomique (CEA)/Direction des Applications Militaires (DAM) site in Bruyères-le-Châtel, France (Attié et al. 2003). We used our MGEANT software (Sturner et al. 2000) to produce high-fidelity Monte Carlo simulations of these calibration runs. MGEANT is a gamma-ray instrument simulation package developed at NASA/GSFC that is based on GEANT 3. It has several benefits over standard GEANT 3 (see `wwwasd.web.cern.ch/wwwasd/geant`). The MGEANT source code contains several beam geometry and spectrum generators that allow users to customize their executable at compile time. The MGEANT releases are available at our website `lheawww.gsfc.nasa.gov/docs/gamcosray/legr/integral`.

Comparisons between the ground calibration and simulated spectra led to improvements in the MGEANT software as well as in the modeling of SPI and the calibration site. This includes improvements to the modeling of the SPI Anti-Coincidence Shield (ACS) and the inclusion of Doppler broadening when simulating Compton scattering by bound electrons through the use of the GLECS add-on package (see `nis-www.lanl.gov/~mkippen/actsim/glecs` for details). A highly detailed computer mass model for SPI and the ground calibration site was developed with particular emphasis on the SPI cryostat including detector modules, preamplifiers, and support structures (see Fig. 1). Much of the SPI mass model was derived from technical drawings provided by various SPI team institutions. A notable exception is the cryostat and its support structure which was translated directly from CAD

Send offprint requests to: S. J. Sturner,
e-mail: `sturner@swati.gsfc.nasa.gov`

⋆ Based on observations with INTEGRAL, an ESA project with instruments and science data center funded by ESA member states (especially the PI countries: Denmark, France, Germany, Italy, Switzerland, Spain), Czech Republic and Poland, and with the participation of Russia and the USA.

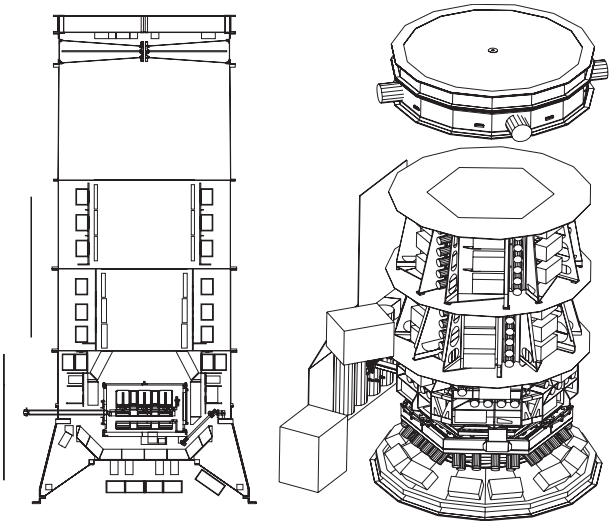

Fig. 1. Shown are two detailed views of the NASA/GSFC SPI computer mass model. On the left is a cut-away view of SPI. On the right is a rendered view of SPI in which the outer support tube has been removed for clarity.

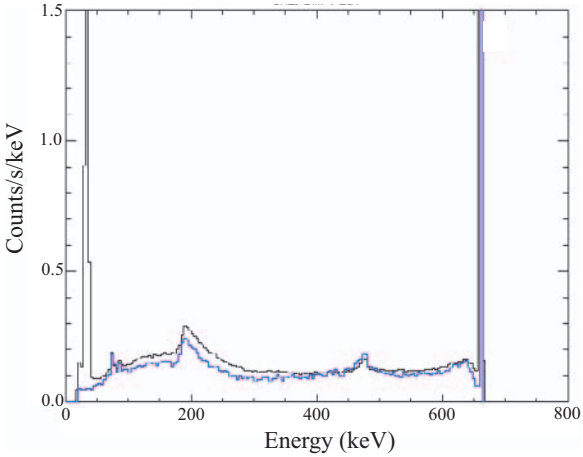

Fig. 2. Comparison of SPI Bruyères-le-Châtel ground calibration data for a ^{137}Cs source (black) and the MGEANT simulation (blue), after MGEANT and mass model improvements, for single detector events summed over the entire camera. Note that the low-energy line seen in the data was not included in the simulation and that the vertical scale has been greatly expanded to exagerate the small differences between the curves. For example, the count rate in the 661−662 keV photopeak bin of the calibration data is ∼31 counts/s. The total counts above 50 keV in the two curves differ by only ∼3%.

files at CEA/Saclay. Once these improvements were made, we achieved a remarkably good agreement between data and simulation (Fig. 2).

We subsequently determined that it was necessary to include mass models for the rest of the INTEGRAL spacecraft, including IBIS and JEM-X, when generating the SPI inflight response. The most important reason for this is that the JEM-X masks are within the partially coded field of view of SPI. Thus the mass model used for generating the SPI responses contains the SPI mass model combined with The INTEGRAL Mass Model (TIMM) developed at the University of Southampton (Ferguson et al. 2003).

3. Method for response generation

We have conducted investigations into methods to reduce both the computation time and storage requirements for the SPI instrument response which is separated into two parts: the imaging response function or IRF and the redistribution matrix file or RMF. The IRFs are a set of FITS files which contain the detector effective area as a function of the detector number, the incident photon direction, and the incident photon energy. The RMFs contain information about the energy distribution of detector counts for photons of a given incident energy.

A full Monte Carlo calculation of the SPI response including the energy-redistribution portion, was determined to be unrealistically CPU and storage intensive. Accurately calculating the energy redistribution portion of the response using such an approach would require good statistics in every count bin for every detector, incident photon direction, and input photon energy. Given the energy and angular resolution of SPI, this would require the simulation of an enormous number of incident photons.

We were able to reduce the number of simulated photons that were necessary by separating the response generation process into 2 parts: a ray tracing part that takes into account radiation processes in the mask and shield, and a Monte Carlo part that takes into account radiation processes in the cryostat and detector modules (Fig. 3). The ray tracing portion reproduces the efficiency modulation on small angular scales produced by the mask and shield with the limitation that an interaction is treated as absorption. This is a reasonable approximation since any scattering that takes place in this portion of the mass model is generally occurring far from the detector array. Thus a photon that scatters there is unlikely to interact in a detector. We then use full Monte Carlo techniques, including an accurate treatment of scattering, to model the interaction of photons once they reach the top of the cryostat. Since Monte Carlo techniques are used for interactions within the detectors, this method is used for the calculation of responses for both single and multiple detector events.

This separation into ray tracing and Monte Carlo portions significantly reduces the overall calculation time because the number of directions for which the Monte Carlo portion is run is greatly reduced. The ray tracing part contains the modulation of the incoming photon beam due to the mask. This requires a fine grid of incidence angles. 0.5° pitch was chosen based on the expected 2−3° angular resolution of SPI. The Monte Carlo portion varies only over larger angular scales and thus need only be calculated on a much coarser angular grid, 5° pitch.

We have further reduced the number of Monte Carlo events required by utilizing symmetries in the detector array and by implementing a decomposition of the IRFs and RMFs. We have found that for a given input photon energy, the shape of the RMF can be well characterized by a linear combination of 3 template shapes whose normalizations are stored in the IRF. These 3 components correspond to the detector response to (1) photopeak events, (2) non-photopeak events that interact first in a detector, and (3) photons that interact first in passive

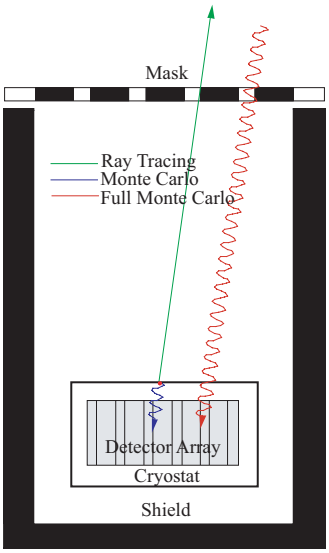

Fig. 3. Schematic illustration of the decomposition of the response generation process into ray tracing and Monte Carlo parts.

material such as the cryostat. These templates, to a good approximation, do not vary with detector or direction, only their normalization changes. Thus once the templates are determined for a given photon energy, it is only the normalization which need be calculated for every direction and detector. This parameterization requires large numbers of events only in each of the 3 components, thus greatly reducing the computation time and storage requirements for the simulated event data. In addition, the RMF decomposition into static components can be exploited in the analysis software leading to a significant reduction of memory use.

The Monte Carlo and ray tracing data sets were created using the MGEANT simulation software. The response generation software then combines this information into a set of IRFs for a range of incident photon energies. The resulting IRFs each contain a four dimensional matrix where the four dimensions are: two angular dimensions (a parameterization of θ and ϕ), a third dimension for the set of detectors, and a fourth dimension for the 3 components. An example of one plane of an IRF is shown in Fig. 4.

4. Correction factors

Once the initial set of IRFs have been generated, a series of multiplicative correction factors are applied. These factors are organized into a set of tables that are used to determine a total correction factor for each element of each IRF.

4.1. Correcting for variations in the Ge crystal mass

The first set of correction factors is to compensate for minor mass differences among the 19 detectors. Given the way in which the detector numbers are referenced within MGEANT, it was necessary to make the detectors identical in the SPI mass model. The masses of the 19 Ge crystals in the actual SPI detectors are known to vary by up to 3.7% about their mean mass of 950.91 g which is used in the mass model. Attié et al. (2003)

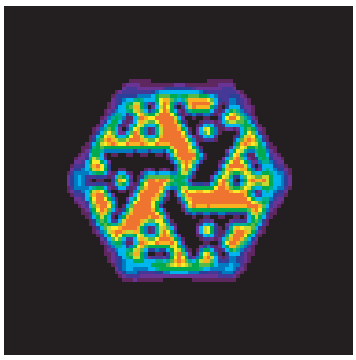

Fig. 4. This illustrates the SPI IRF at 508.33 keV for the photopeak effective area as a function of direction for detector 0. Note that the mask pattern is clearly seen. The hexagonal boundary is a consequence of the shape of SPIÕs BGO collimator.

has shown, using analysis of the Bruyères-le-Châtel calibration data, that variations in individual detector efficiencies about their mean closely follow their variation in mass.

Given the good agreement between detector mass and efficiency variations, the first set of correction factors is merely the ratio of the actual detector Ge crystal mass to their average mass. For cases in which a photon interacts in multiple detectors, the correction factor is the ratio of the average mass for those detectors to the mass used in the model.

4.2. Correcting for simplification of the mask support structure in the mass model

The SPI mask support in the computer mass model is a simplification of the actual support structure. The main part of actual support structure is a honeycomb panel with 1/8 inch diameter hexagonal cells made of NOMEX[1] aramid fiber. In the SPI mass model, this honeycomb panel is replaced by a uniform panel of NOMEX with the same nominal density as the honeycomb. This simplified structure has an average transparency very similar to that of the actual flight model (FM) support panel but the model transparency shows less variation with angle at low energies than does the FM panel (see Fig. 5). To correct for this, we created a table of multiplicative correction factors using measured transparency values and values calculated from the GEANT cross sections and the mass model.

A set of transparency measurements were made on the FM support panel at 17, 21, 31, 35, 59.5, 81, 356, and 511 keV for incidence angles of 0°, 1°, 2°, and 10° from normal (Sánchez et al. 2001). Measurements were performed for a set of 64 different locations on the panel (locations with no tungsten mask elements present) from which a mean transparency was determined for each photon energy and incidence angle. To extend the table to higher photon energies, measurements were also made made using the STM/QM mask support at 898 and 1836.1 keV. We then calculated the transmission of the mass model mask support at these energies and angles. The table of correction factors was then constructed by taking the ratio

[1] NOMEX is a registered trademark of the E. I. du Pont de Nemours and Company.

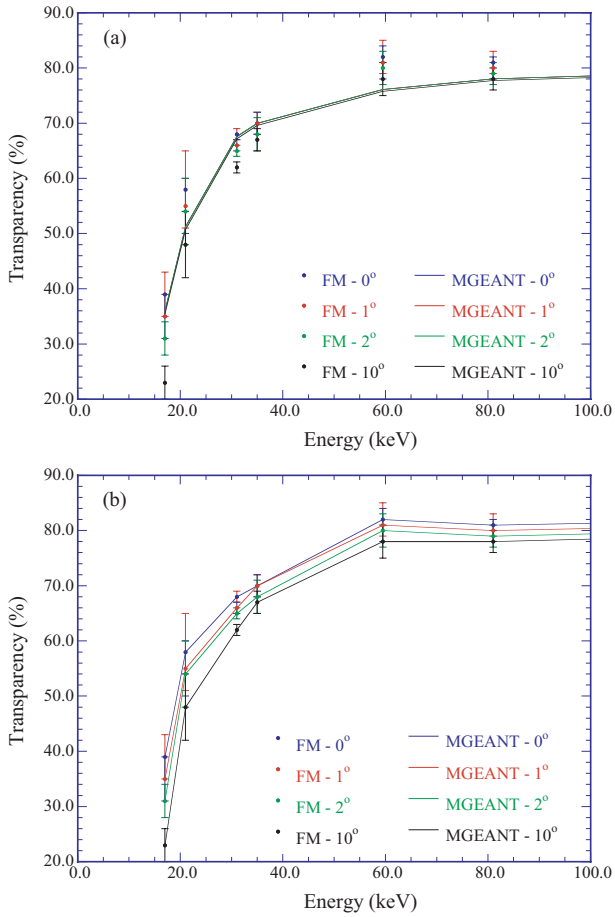

Fig. 5. Comparison of the transparency measurements of the FM honeycomb mask support panel and the transparency calculated for the mass model panel before **a)** and after **b)** corrections were applied. Since the correction factors are merely the ratio of the measured tranparencies to the model transparencies, the corrected model data are, by definition, equal to the measured FM data.

of the measured transparency to the calculated mass model transparency.

4.3. Efficiency correction factors

We have found that the photopeak effective areas in simulations were ∼10% larger than found in the ground calibration data. Thus a table of correction factors was needed to compensate for this difference. The 8 meter source data from the SPI ground calibration were analyzed using the ISDC analysis system including single, double, and triple detector events (Diehl et al. 2003). An effective area was calculated for each of the strong lines from the calibration sources. The same analysis was performed on the simulated data. Ratios of the calibration to simulated effective areas for single, double, and triple detector events were calculated as a function of line energy. These values were averaged over event type and then used as an interpolation grid to calculate the efficiency correction at each IRF energy.

Initial analysis of the ground calibration data was performed only on lines with energies at or above the 59.5 keV line

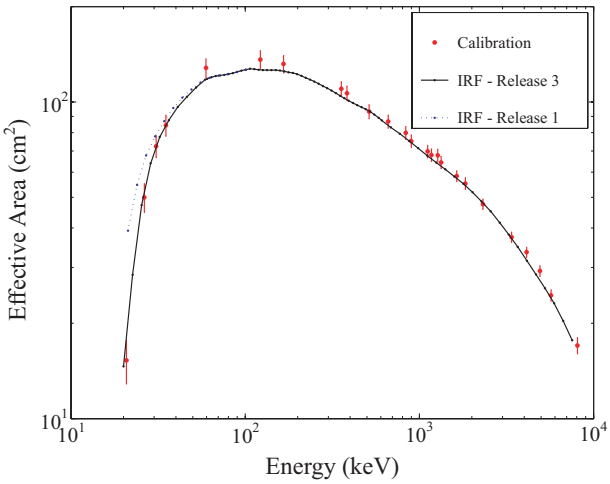

Fig. 6. The SPI camera photopeak effective areas, as contained in the SPI IRFs, for all event multiplicities before (blue) and after (black) the low-energy correction was applied. Releases 1 (Nov. 2002) and 3 (July 2003) of the IRFs correspond to IRF groups spi_irf_grp_0013 and spi_irf_grp_0015 at the ISDC, respectively. Other correction factors discussed in the text have been applied to both IRF data sets. Also shown are the Bruyères-le-Châtel data points of Attié et al. (2003) which have been corrected for absorption by the mask.

from ^{241}Am. The efficiency correction at energies <59.5 keV were initially assumed to be constant at the value for 59.5 keV. We found through analysis of early flight data from the Crab Nebula and pulsar that this assumption was deficient. The SPI efficiency decreases faster than predicted by the simulated response at low energies and thus revised correction factors were needed in the energy range 20−59.5 keV. Additional analyses of weaker, low-energy lines from the Bruyères-le-Châtel ground calibration data were performed (Attié et al. 2003). The new analyses included the 20.80 and 26.35 keV lines from ^{241}Am and the 30.80 and 35.07 keV lines from ^{133}Ba. In Fig. 6 we show the SPI effective area summed over all detectors before and after the revision at low energies.

Periodically throughout the mission, INTEGRAL will continue to make observations of calibration sources such as the Crab Nebula and pulsar in order to perform inflight calibrations of the instruments. We will continue to use these observations to monitor the accuracy of the SPI response and perform updates of the IRFs as needed.

Acknowledgements. The SPI project has been completed under the responsibility and leadership of CNES. We are grateful to ASI, CEA, CNES, DLR, ESA, INTA, NASA, and UCL for their support.

References

Attié, D., Cordier, B., Gros, M., et al. 2003, A&A, 411, L71
Diehl, R., Baby, N., Beckmann, V., et al. 2003, A&A, 411, L117
Ferguson, C., Barlow, E., Bird, A., et al. 2003, A&A, 411, L19
Sánchez, F., Reglero, V., Chato, R., et al. 2001, in Proc. of the 4th INTEGRAL Workshop: Exploring the Gamma-Ray Universe, ed. A. Gimenez, V. Reglero, & C. Winkler (ESA, Noordwijk) 661
Sturner, S. J., Seifert, H., Shrader, C., & Teegarden, B. J. 2000, in Proc. of the Fifth Compton Symp., ed. M. L. McConnell, & J. M. Ryan (AIP, New York), 814